Goddard Earth Observing System chemistry-climate model simulations of stratospheric ozone-temperature coupling between 1950 and 2005

Steven Pawson,[1] Richard S. Stolarski,[2] Anne R. Douglass,[2] Paul A. Newman,[2] J. Eric Nielsen,[1,3] Stacey M. Frith,[2,3] and Mohan L. Gupta[2,4,5]

Received 18 October 2007; revised 7 February 2008; accepted 27 February 2008; published 19 June 2008.

[1] Links between the stratospheric thermal structure and the ozone distribution are explored in the Goddard Earth Observing System chemistry-climate model (CCM). Ozone and temperature fields are validated using estimates based on observations. An experimental strategy is used to explore sensitivities of temperature and ozone using the CCM alongside the underlying general circulation model (GCM) with ozone specified from either observations or from a chemistry-transport model (CTM), which uses the same chemical modules as the CCM. In the CTM, upper stratospheric ozone is biased low compared to observations; GCM experiments reveal that using CTM ozone reduces a warm temperature bias near the stratopause in the GCM, and this improvement is also seen in the CCM. Near 5 hPa, the global-mean ozone profile is biased low in the CTM but is close to observations in the CCM, which suggests that the temperature feedbacks are important in simulating the ozone distribution in the middle stratosphere. In the low stratosphere there is a high bias in simulated ozone, which forces a warm bias in the CCM. The high ozone also leads to an overestimate in total column ozone of several tens of Dobson units in the polar regions. In the late part of the twentieth century the seasonal activation of chlorine, especially over Antarctica, destroys ozone as expected, so that chlorine-induced ozone decreases are overestimated in the CCM compared to the real atmosphere. Ozone-change experiments reveal that the thermal structures of the GCM and CCM respond in a similar manner to ozone differences between 1980 and 2000, with a peak ozone-induced temperature change of about 1.5 K (over 20 years) near the stratopause, which is at the low end of the range computed by other models. Greenhouse-gas-induced cooling increases with altitude and, near the stratopause, contributes an additional 1.3 K to the cooling near 1 hPa between 1980 and 2000. In the Antarctic, the ozone hole is simulated with some success by the CCM. As with many other models, the polar vortex is too persistent in late winter, but counteracting this, the CCM undergoes too much midwinter variability, meaning the ozone hole is more variable than it is in the real atmosphere. Temperature decreases associated with the ozone hole in the CCM are similar to those computed with other models.

Citation: Pawson, S., R. S. Stolarski, A. R. Douglass, P. A. Newman, J. E. Nielsen, S. M. Frith, and M. L. Gupta (2008), Goddard Earth Observing System chemistry-climate model simulations of stratospheric ozone-temperature coupling between 1950 and 2005, *J. Geophys. Res.*, *113*, D12103, doi:10.1029/2007JD009511.

1. Introduction

[2] Interactions among different physical and chemical processes in the stratosphere motivate development of coupled models of ozone chemistry and circulation (chemistry-climate models, CCMs) and their application to numerous questions of relevance to the environment. This study presents Version 1 of the Goddard Earth Observing System (GEOS) CCM and demonstrates some of its strengths and weaknesses as a tool for studies of stratospheric ozone and climate, whose interactions are important but complex.

[1]Global Modeling and Assimilation Office, NASA Goddard Space Flight Center, Greenbelt, Maryland, USA.
[2]Atmospheric Chemistry and Dynamics Branch, NASA Goddard Space Flight Center, Greenbelt, Maryland, USA.
[3]Science Systems and Applications Inc., Lanham, Maryland, USA.
[4]Goddard Earth Sciences and Technology Center, University of Maryland, Baltimore County, Baltimore, Maryland, USA.
[5]Now at Federal Aviation Administration, Washington, D.C., USA.

Copyright 2008 by the American Geophysical Union.
0148-0227/08/2007JD009511

[3] The intent of this study is to evaluate the realism of simulated atmospheric structure over the past five decades. Ability to simulate the past is one important metric in evaluating the suitability of any model for future climate predictions. The study uses model runs forced with "observed" sea-surface temperatures (SSTs) and sea ice distributions, as well as realistic time-dependent emissions of greenhouse gases and halogen-containing compounds. The analysis continues the heritage of evaluating the various components of the GEOS models against observations, using meteorological analyses and ozone observations for evaluation. Alongside the comparison with observations, the study uses ozone from the chemistry-transport model (CTM) and simulations with the parent general circulation model (GCM) to examine the ozone-temperature feedbacks in the system. Where appropriate, this model is discussed in the context of other CCMs.

[4] The CCM includes meteorological and chemical components that have been extensively used for simulations and subject to validation against observations. The GEOS-4 GCM [*Bloom et al.*, 2005] has been used to study aspects of the tropospheric circulation, such as the hydrological cycle [*Bosilovich et al.*, 2005]. The CTM [*Douglass et al.*, 1996] has been used in numerous studies of atmospheric chemistry through which it has been evaluated using aircraft data [e.g., *Considine et al.*, 2003] and space-based observations [e.g., *Douglass et al.*, 2003], using assimilated meteorological fields. The CTM has also been used with meteorological data from a free-running GCM to examine decadal changes in ozone [*Stolarski et al.*, 2006a]. That study was the prelude to the coupling of GEOS-4 GCM and the stratospheric chemistry module as Version 1 of the GEOS CCM.

[5] *Eyring et al.* [2006] evaluated and compared several CCM simulations of the period 1960–2005, including one of the GEOS CCM runs analyzed here. Careful scrutiny of the diagnostics by *Eyring et al.* [2006] reveals that the GEOS CCM simulations agree well with observational estimates in many of the evaluated quantities, spanning the meteorological, transport-related, or reactive chemical diagnostics, in the sense that the results usually lie within the curves representing observational uncertainty and well within the range of results obtained by all models. This study serves to present more details of the GEOS CCM, focusing on realistic and less successful aspects of the simulated ozone and temperature distributions.

[6] Section 2 describes the GEOS CCM, with pointers to its underlying component modules, and summarizes the simulations analyzed in this paper. The mean structure of total ozone is validated against observations in section 3. In section 4 an examination of the coupling between the ozone profiles and the thermal structure is presented: this includes using some GCM simulations with specified ozone distributions from observations and the CTM to help understand the coupling between ozone and temperature in the CCM. This theme of using the GCM to help understand the coupling processes continues in section 5, which examines changes in global ozone and temperature between 1980 and 2000, and section 6 which focuses on the Antarctic ozone hole. The main conclusions are given in section 7, with some discussion of future research directions.

2. Model Heritage, Description, and Runs

[7] This section gives an overview of the GEOS CCM, including some discussion of its heritage from the GEOS-4 GCM and the Goddard CTM. The links with observations, which remain central to NASA's modeling efforts, are emphasized.

2.1. Heritage of the Models

[8] Atmospheric chemistry modeling at GSFC has evolved in unison with NASA's satellite observation programs for trace gases. Data sets such as the long Total Ozone Mapping Spectrometer ozone record and the stratospheric trace gas profiles from the Upper Atmosphere Research Satellite serve two purposes: they provide reference data sets for model validation and they provoke questions about the mechanisms at work in the atmosphere. The Goddard CTM [*Douglass et al.*, 1996] was developed as a tool for middle atmospheric chemistry studies and used prominently in conjunction with UARS satellite data, when it used meteorological fields from successive versions of NASA's GEOS analyses. Using an accurate transport algorithm [*Lin and Rood*, 1996] the CTM can demonstrably represent synoptic-scale features of trace gases in the upper troposphere and stratosphere [*Rood et al.*, 1997]. With analyzed winds, the CTM shows distinct biases in features driven predominantly by an overstrong Brewer-Dobson circulation, such as a low ozone bias in the tropical stratosphere [*Douglass et al.*, 1996, 2003], which are not a problem when using winds from the GCM.

[9] The success of the *Lin and Rood* [1996] transport code in the CTM motivated development of the flux-form semi-Lagrangian "dynamical core" for GCMs. This dynamical core [*Lin*, 2004] retains the conservation properties of the transport code and uses a novel quasi-Lagrangian vertical coordinate [*Lin and Rood*, 1997] that allows for accurate computation of vertical motions. The dynamical core has been used in several GCMs, including the "AMTRAC" chemistry-climate model [*Austin and Wilson*, 2006]. Use of the *Lin* [2004] dynamical core in the GEOS CCM is one of the main factors that lead to successful transport characteristics, evidenced by the "tape recorder" signal and the age-of-air distribution in the work of *Eyring et al.* [2006], and by realistic particle dispersion characteristics [*Schoeberl et al.*, 2003].

[10] Simulations of the global water cycle [*Bosilovich et al.*, 2005] have revealed that the GEOS-4 GCM can give meaningful information on the global transport and cycling of moisture in the troposphere. *Charlton et al.* [2007] examined Arctic sudden warmings in a 50-year simulation (1950–2000) of the GEOS-4 GCM, showing that the model generates early-winter, midwinter, and late-winter warmings with approximately the same frequency as the real atmosphere, with some tendency for late vortex breakdowns. *Olsen et al.* [2007] used the model to isolate the sensitivity to SSTs of stratosphere-to-troposphere exchange (STE) of mass and ozone. The GEOS-4 version used in this study (GEOS-4.0.3) differs slightly from GEOS-4.0.2, with a different land-surface model [see *Bloom et al.*, 2005] and

Table 1. List of the Time-Slice Runs Performed With the GEOS-4 GCM[a]

Run	Period	Specified Ozone
G1980/OBSO3	12 × 1980	observed, 1980 [*Langematz et al.*, 2003]
G2000/OBSO3	12 × 2000	observed, 2000 [*Langematz et al.*, 2003]
G1980/CTMO3	12 × 1980	CTM, 1980 [*Stolarski et al.*, 2006a]
G2000/CTMO3	12 × 2000	CTM, 2000 [*Stolarski et al.*, 2006a]

[a]The columns show the name of the run, the period covered, and the sources of the specified ozone. All runs used a fixed CO_2 distribution of 355 ppmv and identical sea-surface temperature and ice and distributions.

some minor changes to the convection code: neither of these changes has a substantial impact on the stratosphere.

2.2. GEOS-4 GCM: Description and Runs

[11] The flux-form semi-Lagrangian dynamical core with a floating vertical coordinate [*Lin*, 2004] computes the dynamical tendencies of vorticity, divergence, a thermodynamic variable, surface pressure and any number of trace constituents in GEOS-4. The dynamical time step is 7.5 minutes. Spatial resolution is flexible, but in all simulations discussed here it was 2.5° × 2° (longitude by latitude) with 55 layers bounded by the surface and a top-edge boundary at 0.01 hPa (near 80 km). The upper boundary condition specifies no flow out of the model domain (i.e., $\omega = 0$ at the top edge).

[12] Remapping from the floating vertical coordinate to a standard hybrid sigma-pressure ("eta") grid [*Simmons and Strüfing*, 1983] is performed every time the physical parameterization package is run, selected to be every 30 minutes. The representations of subgrid moist physics and radiation are adapted from *Kiehl et al.* [1998], as described by *Bosilovich et al.* [2005]. Mountain-forced gravity-wave drag is specified after *Kiehl et al.* [1998], with the addition of a coarsely resolved spectrum of waves with nonzero phase speeds [*Garcia and Solomon*, 1985] to account for other sources that are important in the middle atmosphere.

[13] The energy and water balance at the land surface are determined interactively using a physical land model [see *Bosilovich et al.*, 2005]. The model accounts for ice and snow accumulation when computing energy and moisture transfer between land and atmosphere.

[14] At the ocean surface, temperature and sea ice distributions are specified using a global data set. All of the runs in this work specified SST and sea-ice distributions from the "HadISST" (Hadley Centre Ice and Sea-Surface Temperature) data set of *Rayner et al.* [2003].

[15] Four time-slice runs of the GEOS-4 GCM with specified ozone (Table 1) are used to help interpret the ozone feedbacks in the CCM. To eliminate impacts of climate change on the circulation, all four GCM runs used identical greenhouse-gas (GHG) distributions, with a CO_2 mixing ratio of 355 ppmv, and the same time series (1988–2000) of SST and ice. Runs G1980/OBSO3 and G2000/OBSO3 use estimates of ozone (for 1980 and 2000) based on observations [*Langematz et al.*, 2003]. Runs G1980/CTMO3 and G2000/CTMO3 use ozone (averages for 1978–1982 and 1998–2002) simulated by the Goddard CTM [*Stolarski et al.*, 2006a]. Each run consists of a 2-year spin-up period followed by 10 years used for science evaluation. The four runs serve two purposes. First, the impact of replacing observed ozone with values from the CTM provides an intermediate step for the CCM, where ozone and temperature are calculated interactively. Second, using ozone values for 1980 and 2000 facilitates examination of how ozone change impacts the modeled temperature (as in the work of *Langematz* [2000]).

2.3. GEOS CCM: Description and Runs

[16] Version 1 of the GEOS CCM comprises the physical processes from the GEOS-4 GCM and a set of chemical reactions that describe the composition of the stratosphere. Tropospheric ozone is represented in a simple manner, with relaxation to the climatology of *Logan* [1999]. Gases with surface sources are specified as mixing ratios at the lowest model layer. Surface-layer concentrations of "greenhouse gases" and "ozone-depleting gases" are specified: in all runs discussed here, established emission inventories are used. Moisture distributions are controlled by the GCM physical processes in the troposphere [*Kiehl et al.*, 1998] and by chemical processes in the stratosphere.

[17] The photochemistry code is based on the family approach, as described by *Douglass and Kawa* [1999] and is updated to include reaction rates and cross section data from the Jet Propulsion Laboratory Evaluation 14 [*Sander et al.*, 2003]. A total of 35 trace gases are transported in the model. Processes involving polar stratospheric clouds use the parameterization described by *Considine et al.* [2000]. Additional reactions are added to the mesosphere, in order to balance the moisture and methane budgets (without this, too little moisture would be generated in the mesosphere).

[18] The coupling between the chemical and physical state of the atmosphere proceeds directly through the GCM's radiation code. The predicted distributions of H_2O, CO_2, O_3, CH_4, N_2O, CFC-11, and CFC-12 are used in the radiation computations.

[19] The main focus of this work is the evaluation of two "transient" GEOS CCM runs (Table 2). The two runs are identical except that they start with a different initial condition: this two-member ensemble was run to provide some degree of statistical confidence in the results. The runs were forced using HadISST [*Rayner et al.*, 2003] SST and sea ice distributions. Standard scenarios of greenhouse gases (GHG) and ozone-depleting substances [*World Meteorological Organization*, 2003; *Eyring et al.*, 2006] were specified as mixing ratios in the lowest model layer; this specification ensures that lower tropospheric distributions of these gases follows the observed record in the past. The first run, P1, began in January 1950 from a previously spun-up GCM run and zonal-mean climatologies of constituent distributions. (Run P1 was used in the work of *Eyring et al.* [2006].) The atmospheric state from 1 January 1951 of run P1 was used to initialize the second run, P2, on 1 January 1950: the perturbation occurs because of the mismatch between the atmospheric state and the boundary conditions. (The acronyms P1 and P2 refer to "Past" climate simulations numbers 1 and 2.)

[20] A third simulation of the 1951–2005 period was also performed, in order to help separate the impacts of GHG and CFCs on ozone and the thermal structure. Denoted Cl1960, this run was identical to P2, except that all chlorine-containing trace gases were fixed at their 1960 values.

Table 2. List of the GEOS CCM Runs Used in the Study, Along With Some Details of Their Formulation[a]

Run	Period	Initialization	SST/Ice	GHG Emission	CFC Emission
P1	1950–2005 (transient)	1 Jan. 1950, climatology	HadISST, 1950–2005	observed, 1950–2005	observed, 1950–2005
P2	1951–2005 (transient)	1 Jan. 1951 (P1)	HadISST, 1950–2005	observed, 1950–2005	observed, 1950–2005
Cl1960	1951–2005 (transient)	1 Jan. 1951 (P1)	HadISST, 1950–2005	observed, 1950–2005	observed, 1950–1960
T1980	25 × 1980 (time slice)	1 Jan. 1975 (P1)	HadISST, 1979–2004	observed, 1975	observed, 1975
T2000	25 × 2000 (time slice)	1 Jan. 1995 (P1)	HadISST, 1979–2004	observed, 1995	observed, 1995

[a]The table columns give the run name, the period spanned, the initial state used, the SST/ice scenario boundary condition, the GHG emissions, and the CFC emissions used in the runs. HadISST, Hadley Centre Ice and Sea-Surface Temperature data set.

[21] To assist interpretations of the transient runs, two "time-slice" integrations of the GEOS CCM have been performed. The two runs are denoted "T1980" and "T2000" and intended to give stable estimates of the mean atmospheric state for prevalent stratospheric chemical loadings in 1980 and 2000. These two runs are identical, except for the specification of constituent mixing ratios at the lower boundary. The T1980 run used surface mixing ratios appropriate for 1975, while T2000 used values for 1995: this 5-year delay is intended to approximately account for the transport-induced time lag between tropospheric and stratospheric constituents. The same time series (1979–2004) of SST and ice was used in each run, even though they use different GHG distributions. This decision was made with two competing demands: the first was to ensure that the only differences between the simulations were those forced directly by the change in composition of the atmosphere; the second, which was deemed less important for these experiments, was the knowledge that SSTs rise as the atmospheric GHG loading increases, which means the modeled atmosphere is possibly out of balance with the underlying boundary. An alternate approach would have been to repeat a single year of SST data each year of the model run: this experimental configuration was not chosen because some early model runs suggested that year-to-year SST variations do impact the middle atmospheric circulation [see also *Braesicke and Pyle*, 2004; *Sassi et al.*, 2004].

3. Validation of Total Ozone

[22] Ozone is the major link between stratospheric chemistry and climate. Its distribution arises from the complex interactions between transport and temperature-dependent photochemistry, where the temperature (and to some extent the transport) depend on the radiative effects of ozone. The success of the ozone simulation is thus an integral metric for the CCM. This evaluation of the total ozone in the GEOS CCM uses databases for total ozone based on global satellite observations [*Stolarski and Frith*, 2006] and a ground-based network [*Fioletov et al.*, 2002].

[23] The zonal-mean, annual-mean total ozone column in GEOS CCM, averaged over 1995–2004, agrees well with both ground-based and space-based observations in the Tropics (Figure 1). It is around 5 DU lower than the space-based observations suggest, but close to the ground-based data (which are sparse [*Fioletov et al.*, 2002]). In the northern hemisphere the simulated ozone increases toward

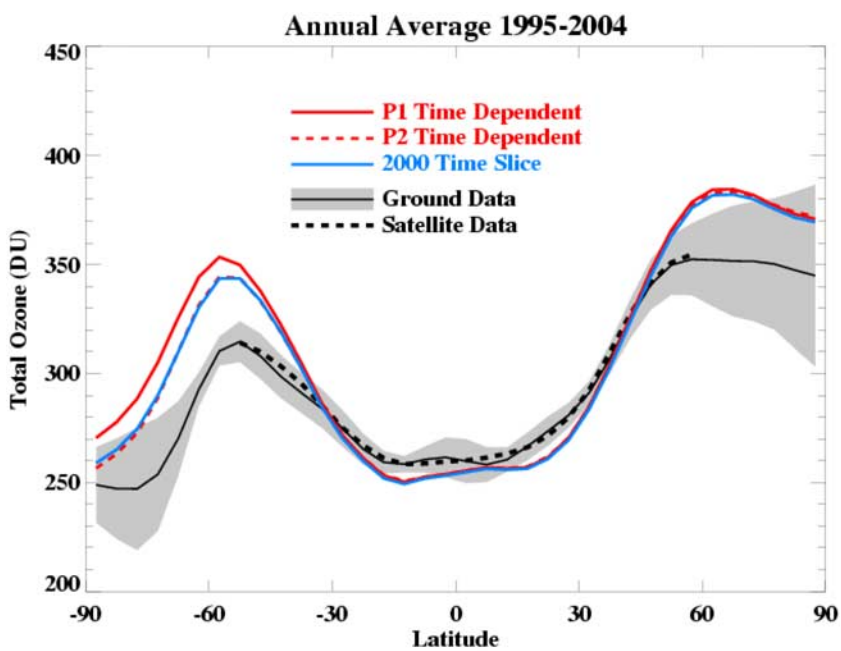

Figure 1. The latitudinal structure of zonal-mean, annual-mean total ozone for 1995–2004. The curves show data from ground-based observations (black solid curve with 2-sigma error bar), from space-based data (black dashed curve), and from three model simulations: P1 (red solid curve), P2 (red dashed curve), and T2000 (blue solid curve).

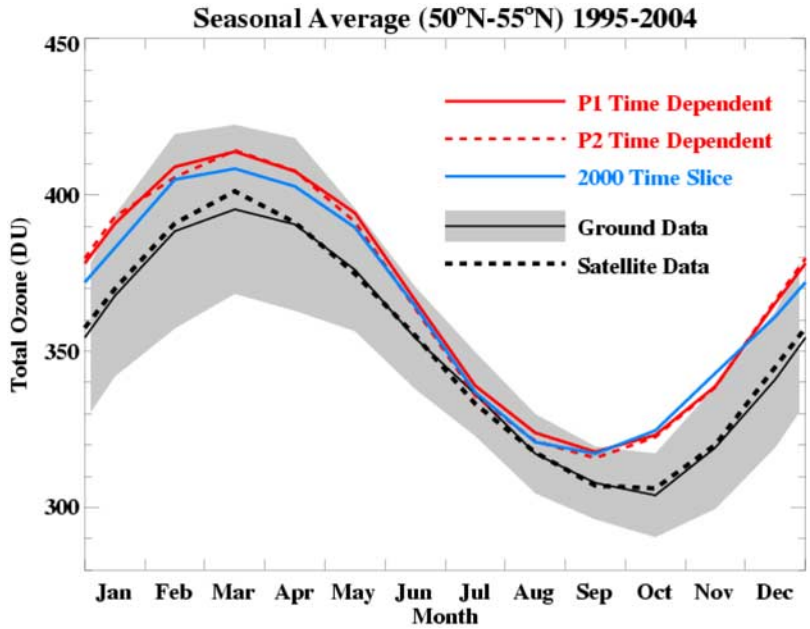

Figure 2. Time series showing the monthly averaged total ozone for the 50°–55°N latitude band averaged for 1995–2004. The curves show data from ground-based observations (black solid curve with 2-sigma error bar), from space-based data (black dashed curve), and from three model simulations: P1 (red solid curve), P2 (red dashed curve), and T2000 (blue solid curve).

about 60°N, in accord with the observations, but peaks near 385 DU, which is more than 30 DU too high. Similarly, in the Southern Hemisphere the latitudinal dependence is well captured, with a peak near 50°S and a subsequent decrease toward the Pole, but the simulated values are around 30 DU higher than the observations. There are some differences among the simulations in the Antarctic region, with run P1 showing a higher bias than run P2 and the time-slice simulation T2000: these arise from year-to-year variations in the strength of the simulated ozone hole.

[24] To illustrate the ability of the GEOS CCM to capture the seasonal cycle in total ozone, Figure 2 shows time series of monthly-mean total ozone in the 50°–55°N latitude band from the two sets of observations and the three simulations. The high bias in the simulated ozone persists through most of the year, but it is very small in July and August. This seasonal anomaly grows when the summertime decrease of ozone in the CCM levels out in late August at about 12 DU above the minimum reached in October in the real atmosphere. The high bias that sets in late summer is maintained throughout the winter and early spring. The simulation then exhibits a seasonal decrease that is 40% greater than the observations over the two months from middle May to middle July.

[25] In summary, this evaluation shows that the GEOS CCM simulates the latitudinal distribution of zonal-mean ozone with a high bias at high latitudes. While the seasonal cycle is broadly correct, the model fails to capture the fall minimum at northern middle latitudes.

4. Thermal Structure and Its Dependence on Ozone

[26] Temperature near 100 hPa is an important metric in chemistry-climate modeling. First, since it is near the tropical tropopause it indicates the success of the model in capturing the transition between convective-radiative and chemical-radiative control of temperature [e.g., *Fels et al.*, 1980]. Second, tropical tropopause temperatures impact the moisture budget of the stratosphere [e.g., *Holton et al.*, 1995]. Third, this is the layer of transition between tropospheric warming and stratospheric cooling as greenhouse gases increase, where the direct radiative impacts of GHG and ozone change are important [e.g., *Ramaswamy and Schwarzkopf*, 2002; *Santer et al.*, 2003]. Fourth, it is the altitude region where ozone change has its largest impacts on radiative forcing of surface climate [e.g., *Forster and Shine*, 1997].

[27] Figure 3 demonstrates the success of the CCM in capturing the zonal-mean 100-hPa temperature for January in the period 1995–2004. Runs P1 and P2 differ by less than 0.4 K at each latitude, so P2 is not shown. In the Tropics, differences between run P1 and observations are within tenths of a degree. The model displays a strong cold bias approaching 10 K at the South Pole, which is a common and as-yet unexplained feature of almost all climate models in the polar summertime [*Boer et al.*, 1992]. At northern high latitudes the wintertime variability leads to a dipolar structure in differences (−4.1 K at the North Pole and 1.8 K at 50°N).

[28] *Pawson et al.* [2000] showed that the global-mean stratospheric temperature was biased cold in almost all GCMs at that time. This bias was attributed to the radiation transfer codes used in the models or to other components such as the imposed ozone climatology. *Eyring et al.* [2006] found that most "2006-era" CCMs are in better agreement with observations than the "2000-era" GCMs. They attributed this improvement to improvements to the radiation codes and to the coupling of ozone into the prediction. This issue is examined in the present model.

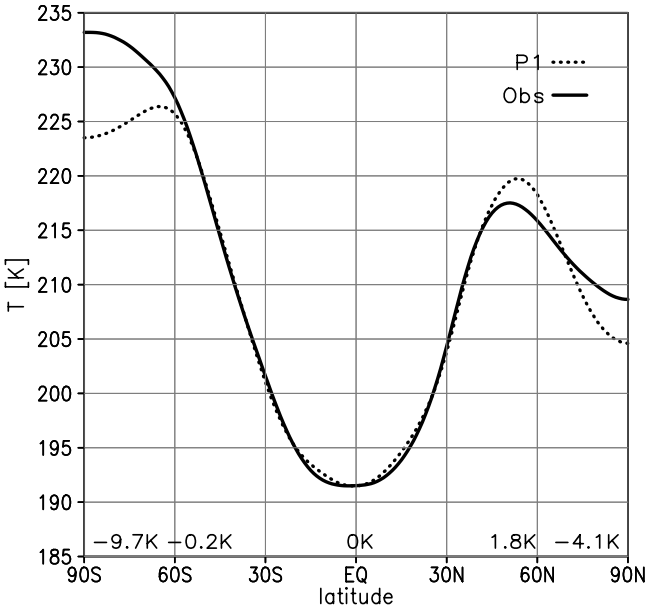

Figure 3. The meridional structure of the zonal-mean temperature at 100 hPa in January, averaged over 1995–2004. The curves show data from GEOS-4 reanalyses (solid curve) and model run P1 (dotted curve). The numerical values are the differences between run P1 and the analyses at the South Pole, 50°S, the Equator, 50°N, and the North Pole.

[29] Figure 4 compares the global-mean temperature in January 1995–2004 in run P1 to meteorological analyses (GEOS-4). Global temperatures in run P2 are almost identical to P1 and January is representative of all months. There is agreement to within tenths of a degree throughout the troposphere. Between 100h Pa and 20 hPa, the CCM has a warm bias that peaks at 3.6 K at 50 hPa. Above this there is a cold bias that peaks at −3.2 K at 5 hPa. (The lack of in situ temperature observations leads to some uncertainty in the analyses in the upper stratosphere.) Figure 4 reiterates the conclusion of *Eyring et al.* [2006] that current CCMs do not show a cold bias through the stratosphere; possible causes of the height-dependent temperature biases will now be examined.

[30] One important question is the extent to which the use of a chemically interactive ozone distribution impacts the thermal structure of the model. *De Grandpré et al.* [2000] gave an example of this. They found that introducing ozone chemistry into the Canadian Climate Model substantially reduced a high-temperature bias at the summer stratopause that occurred in their GCM with specified ozone. *Sassi et al.* [2005] also examined the thermal response to coupling ozone chemistry into a GCM, isolating strong temperature responses to ozone in the high stratosphere and mesosphere. The feedback is examined for the present model.

[31] Global-mean, 10-year mean temperatures for three 1980 time-slice runs (Figure 5) reveal differences in the stratosphere, where ozone is predicted in CCM run T1980 and specified, from the CTM or observations, in GCM runs G1980/CTMO3 and G1980/OBSO3. Near 1 hPa, run T1980 lies between the others, following G1980/CTMO3 more closely in the lower mesosphere. Results from the 2000 time-slice runs are similar, but because 1980 GHG concentrations were used in runs G2000/OBSO3 and G2000/CTMO3, there is a discrepancy in comparing these to run T2000. Given the realism of 1 hPa temperature in run P1 (Figure 4), this result supports that of *de Grandpré et al.* [2000]: the interactive chemistry improves the simulated temperature near the stratopause in the GEOS CCM.

[32] Figure 6 shows global-mean ozone profiles in January from observations [*Langematz et al.*, 2003], the CTM [*Stolarski et al.*, 2006a] and run T1980 of the CCM. This plot reveals height-dependent biases in the simulated ozone. There is too little ozone in the upper stratosphere of the CTM and the CCM. The peak mixing ratios agree more closely with observations in the CCM than in the CTM, but the profile is displaced downward. (The vertical shift in peak mixing ratios is comparable to the vertical resolution of the data used to construct the climatology.) Between 100 and 10 hPa, there is more ozone in the simulations than in the observations. Aspects of the ozone-temperature coupling are now discussed.

[33] Comparison of global-mean solar and longwave radiative heating rate differences between GCM runs G2000/OBSO3 and G2000/CTMO3 (Figure 7) illustrates the direct impact of the upper stratospheric ozone bias on the simulated temperature. The weaker solar heating near the stratopause using modeled ozone leads to a lower temperature, which is

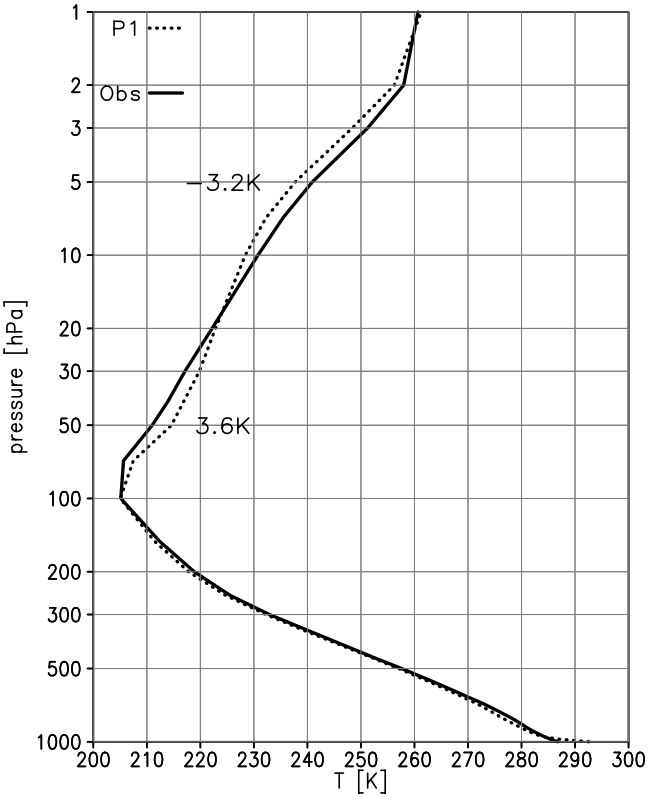

Figure 4. Global-mean temperature profiles in January, averaged for 1995–2004, from the surface to 1 hPa. The (solid) observations curve is from GEOS-4 reanalyses, and data from model run P1 are shown by the dotted curve. The numerical values indicate the model-analysis differences at 50 and 5 hPa.

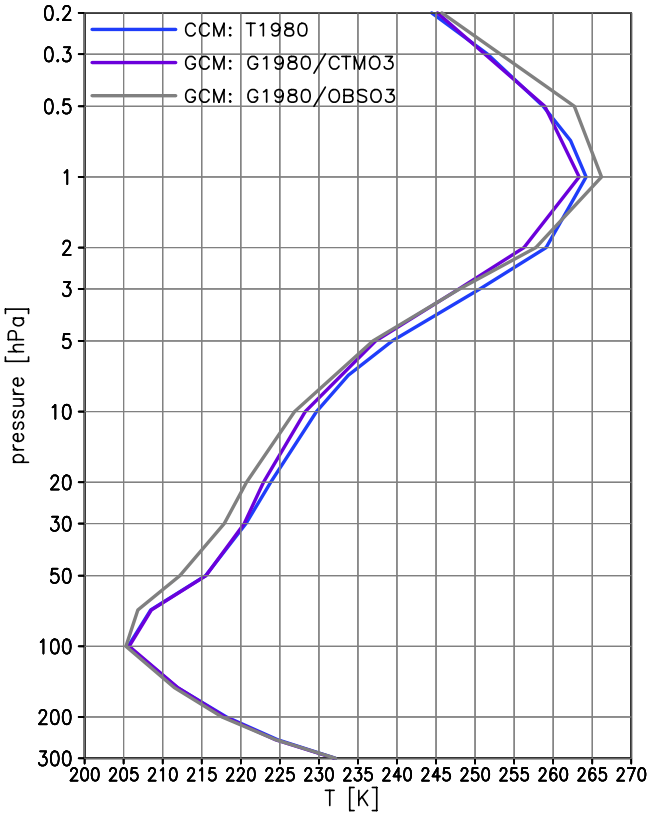

Figure 5. Global-mean temperature profiles between 300 and 0.2 hPa in January from three time-slice integrations for 1980 conditions. The blue curve is the 20-year mean for the T1980 simulation of GEOS chemistry-climate model (CCM). The other two curves show GEOS-4 general circulation model (GCM) simulations using imposed zonal-mean ozone from observations (G1980/OBSO3: gray curve) and the chemistry-transport model (CTM) (G1980/CTMO3: violet curve).

more realistic (Figure 4); this in turn leads to weaker cooling. The GCM experiments illustrate that the low bias in modeled upper stratospheric ozone leads to a more realistic stratopause temperature in the CCM (Figure 4). These results indicate that there is a discrepancy between observations of ozone and temperature in the stratopause region and our ability to model them correctly. Using observed ozone, simulated stratopause temperatures are warmer than those in meteorological analyses. Using low-biased simulated ozone leads to more realistic temperatures. Ozone from the CCM is very similar to that from the CTM, indicating that the global-mean ozone distribution near the stratopause depends only weakly on temperature.

[34] In the lower stratosphere, the connection between ozone and temperature is somewhat similar. The high bias in simulated ozone (Figure 6) leads to the high-temperature bias between 100 and 20 hPa in runs P1 and P2 (Figure 4). In this layer, the GCM runs that use observed ozone in the radiation code (G1980/OBSO3 and G2000/OBSO3) are several degrees cooler than the GCM runs with modeled ozone. At 50 hPa, run G1980/OBSO3 is 3.2 K colder than run T1980 (Figure 5), and run G2000/OBSO3 is 3.8 K colder than T2000. Radiative-heating rate differences show stronger solar heating in the 60-5 hPa layer in run G1980/CTMO3 than in G1980/OBSO3, providing a direct source for the increased temperature there. However, solar-heating rate changes do not explain the higher temperature between 100 and 50 hPa. In this region, the absorption of upwelling radiation in the 9.6-micron ozone bands plays a major role in the thermal balance of the stratosphere [*Hitschfeld and Houghton*, 1961]. The Earth's surface emits strongly in these bands, which are transmitted through the cloud-free troposphere. *Pawson* [1992] showed that changes of several tenths of one degree per day in lower stratospheric radiative-heating rates caused by uncertainty in upwelling fluxes near 9.6 microns lead to differences of several degrees in the modeled temperature. (The large thermal response is because of the long radiative relaxation timescales in the tropical low stratosphere.) Figure 8 shows solar and longwave-heating rates at 70 hPa in January in the GCM runs G1980/CTMO3 and G1980/OBSO3. There are small differences in solar-heating rates that largely cancel out in the global average (Figure 7), with larger differences, of around 0.1 K/d, in the longwave heating in the Tropics. The small difference in total heating in the tropical lower stratosphere, coupled with the extremely long radiative relaxation timescale in this region, leads to the temperature sensitivity here.

[35] To summarize, the coupling of ozone has a beneficial impact on the thermal structure near the stratopause, as in

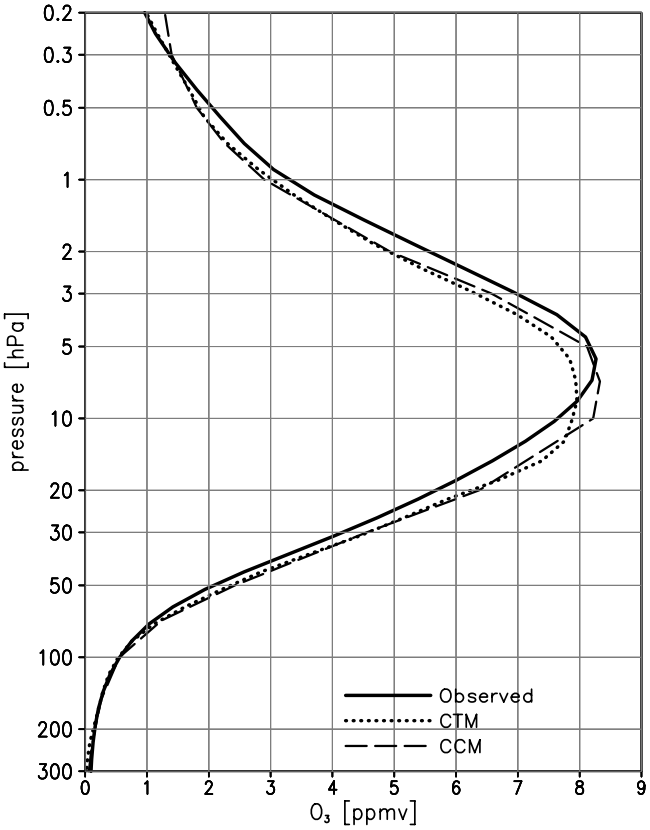

Figure 6. The global-mean ozone profile between 300 and 0.2 hPa in January 1980 from observations (solid curve: *Langematz et al.* [2003]), used in run G1980/OBSO3, from the CTM run (dotted curve: *Stolarski et al.* [2006a]), used in run G1980/CTMO3, and the T1980 CCM (dashed curve).

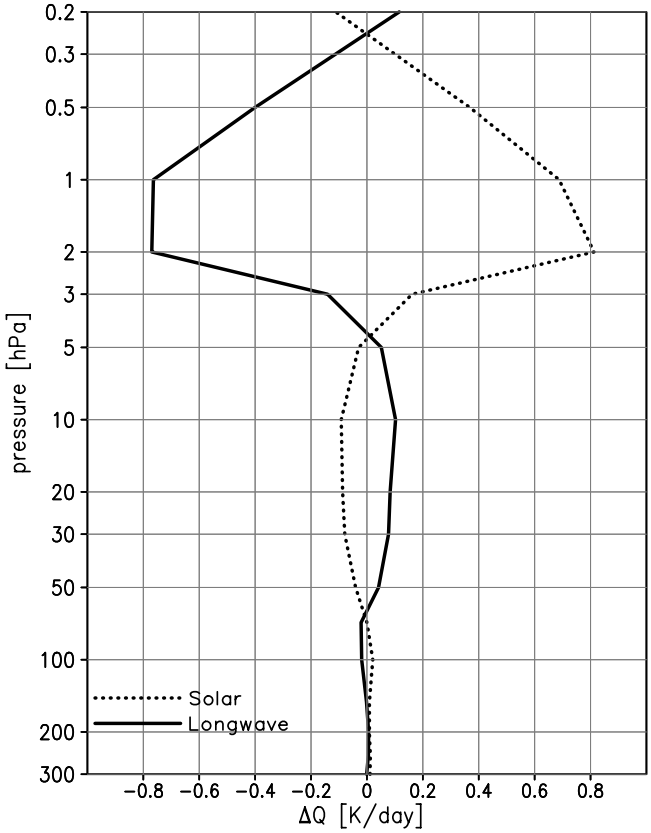

Figure 7. Profiles of global-mean radiative-heating rate differences in January between runs G2000/OBSO3 and G2000/CTMO3. These curves illustrate the impact of using CTM ozone instead of observed ozone in the GEOS-4 GCM. The solar-heating differences are shown with the dotted curve; longwave-heating rate differences are shown with the solid curve.

the work of *de Grandpré et al.* [2000]. However, this beneficial impact on temperature comes with the caveat that ozone is biased low near the stratopause in the CCM. Similarly, the high ozone bias in the low stratosphere leads to a warm bias caused partly by increased solar heating and partly (in the lowermost tropical stratosphere) by increased absorption of upwelling radiation at 9.6 microns. These results emphasize the importance of ozone as it directly controls the stratospheric temperature structure. In the middle stratosphere, the coupling benefits the ozone distribution.

5. Global Ozone and Temperature Change: 1980–2000

[36] Several prior studies have examined the stratospheric temperature response to ozone change. By imposing an ozone change derived from observations on the Berlin GCM, *Langematz* [2000] demonstrated that the reduction in solar heating leads to a peak thermal response near the stratopause. Various estimates of the middle atmospheric cooling arising from ozone decreases between 1980 and 2000 show values of around 1–2.5 K per decade near the stratopause, depending on the model used and the precise period investigated [*Rosier and Shine*, 2000; *Langematz et al.*, 2003; *Hare et al.*, 2004; *Braesicke et al.*, 2006]. This section examines ozone- and GHG-induced temperature changes in the GEOS-4 GCM and the GEOS CCM. The response of the GEOS-4 GCM to imposed ozone changes allows comparisons with prior publications. Following this, the feedbacks between ozone change and temperature change in the GEOS CCM are discussed.

[37] Runs G1980/OBSO3 and G2000/OBSO3 used the same ozone distributions as those of *Langematz et al.* [2003]. The global-mean ozone concentration decreases throughout the stratosphere between 1980 and 2000 (Figure 9). This leads to a decrease in temperature, with peak decreases of about 0.8 K near 70 hPa and more than 2 K at 0.5 hPa (Figure 10). This profile has a similar shape to that computed by *Langematz et al.* [2003] and *Hare et al.* [2004], but the maximum cooling near the stratopause is less than the 1.5–2 K/decade computed in those studies. The cooling is closer to that computed by *Braesicke et al.* [2006], who imposed a similar ozone change.

[38] The GCM runs G1980/CTMO3 and G2000/CTMO3 used zonal-mean ozone distributions from the CTM [*Stolarski et al.*, 2006a]. The global-mean ozone change is similar to that deduced from observations, except the peak decrease near the stratopause is larger and there is less depletion in the lower mesosphere, where the chemistry is computed less accurately in the CTM (Figure 9). (There are some seasonal variations in this. In July the peak ozone change near 3 hPa in the CTM is smaller than that deduced from observations.) This ozone change leads to a broadly similar profile of 1980–2000 temperature change in the GCM (Figure 10) as with the observed ozone, despite the mean temperature bias between runs G1980/CTMO3 and

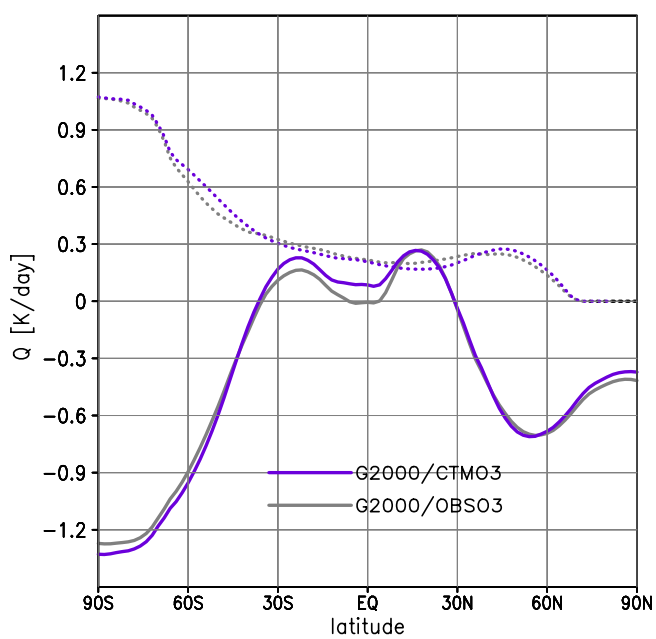

Figure 8. Zonal-mean radiative-heating rates (K/d) as a function of latitude at 70 hPa in January for the GCM runs G2000/CTMO3 (violet curve) and G2000/OBSO3 (gray curve). Solar-heating rates are dotted, and longwave-heating rates are solid.

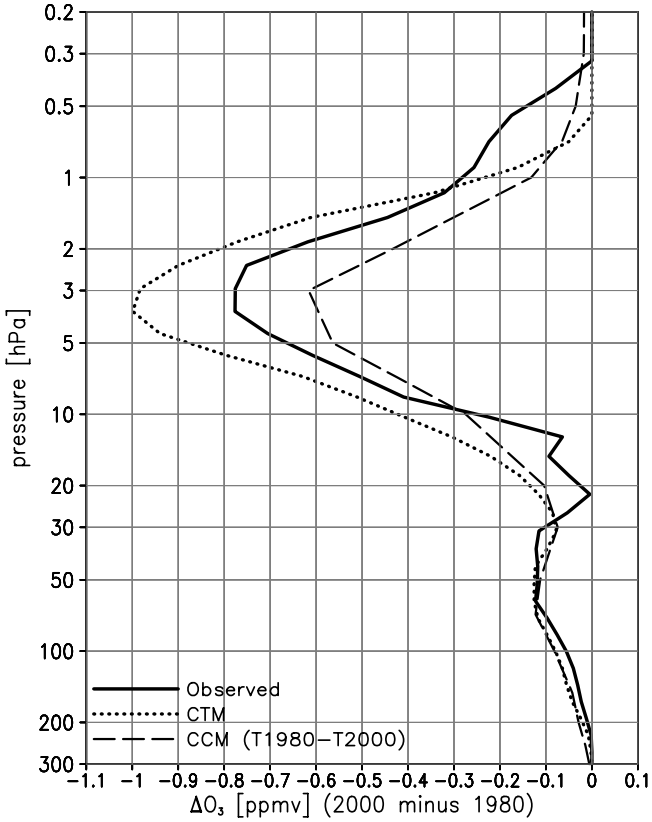

Figure 9. The global-mean ozone change in January between 2000 and 1980, deduced from observations [*Langematz et al.*, 2003] (solid curve), simulated in the CTM [*Stolarski et al.*, 2006a] (dotted curve), and simulated in the time-slice integrations of the GEOS CCM (T2000 minus T1980, dashed curve).

G1980/OBSO3. The peak cooling of 2.3 K over two decades is located near 2 hPa, and there is less cooling in the low mesosphere than in the runs with observed ozone.

[39] The discussion so far confirms that the ozone changes computed by the CTM are in reasonable agreement with observations and that the GCM responds to these imposed ozone changes in a manner that is consistent with previous model studies, although the thermal response to the ozone change is on the low side of the range exhibited by earlier models. Attention is now given to the temperature changes in the CCM runs (Figure 11), which include GHG changes as well as ozone change, meaning that there is more cooling through most of the stratosphere than in the GCM runs.

[40] Figure 11 shows the global-mean temperature changes in January between 1980 and 2000 in the CCM runs. The 1980–2000 temperature change in the time-slice runs (blue curve) is based on 20-year averages. The cooling increases with altitude above the tropopause, peaking at slightly less than 3 K near 1–2 hPa, and then decreases in the mesosphere. This result is statistically robust, since the differences in both temperature and ozone are more than three times larger than the spread in the range of values attained in the T2000 and T1980 runs. Peak temperature changes between 1980 and 2000 in runs P1 and P2 are slightly smaller than in the time-slice runs, but have similar structure. For this purpose, the 1980 and 2000 states are the 10-year averages over 1975–1984 and 1995–2004.

[41] Because chlorine is fixed in run Cl1960, the temperature change there is primarily due to GHG increases (excluding the CFCs). Above 30 hPa, the direct GHG-induced cooling dominates the temperature change in Cl1960 and changes near 1 hPa are about 1.3 K over the two decades (Figure 11). Assuming that GHG- and ozone-induced temperature decreases are approximately linear in the stratosphere, subtracting the GHG-induced cooling (run Cl1960) from the total cooling in runs P1 and P2 yields an estimated contribution of ozone loss to the cooling. This shows peak values of between 1.2–1.5 K at 2 hPa (red curves in Figure 11). This implies that there is less ozone-induced cooling between 1980 and 2000 in the CCM than in the GEOS-4 GCM runs (e.g., the temperature change at 2 hPa is 1.5 K in P2-Cl1960 and 2.3 K in G2000/CTMO3-G1980/CTMO3). This reduced temperature change is consistent with the smaller reduction in ozone between 1980 and 2000 in the CCM than in the CTM.

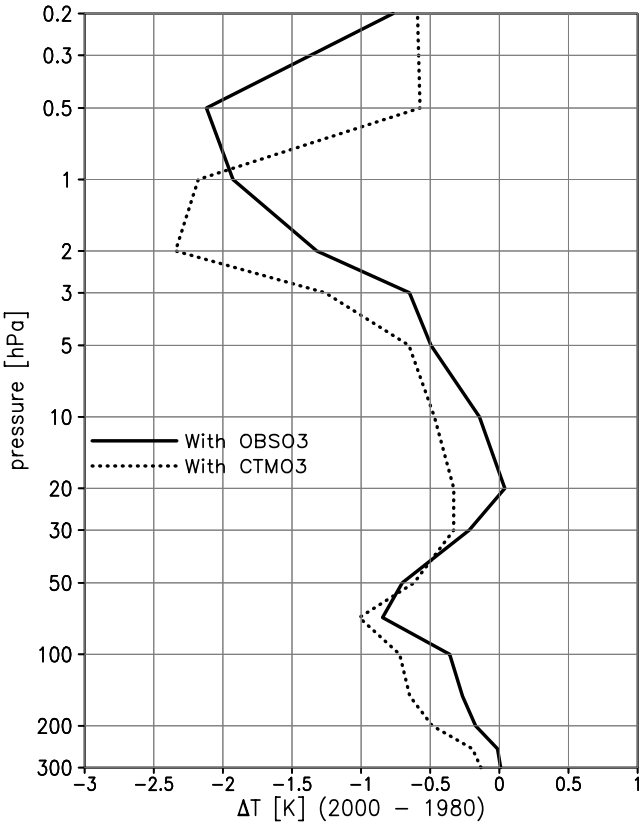

Figure 10. Global-mean temperature change between 1980 and 2000 for the two pairs of GEOS-4 GCM integrations with imposed ozone. The dotted curve is for the GEOS-4 GCM with ozone imposed from the CTM (G2000/CTMO3 minus G1980/CTMO3). The solid curve is for the GEOS-4 GCM with ozone imposed from observations (G2000/OBSO3 minus G1980/OBSO3). Greenhouse-gas (GHG) concentrations and sea-surface temperatures (SSTs) were identical in these simulations.

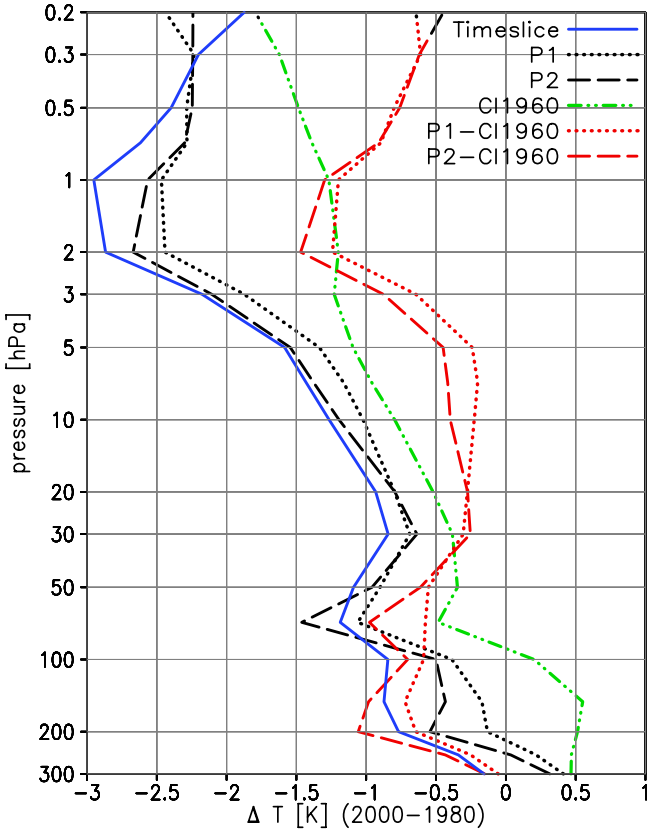

Figure 11. The global-mean temperature change between 1980 and 2000 in the GEOS CCM simulations. The blue solid curve shows the 20-year mean change between time-slice runs T1980 and T2000. The black curves show the changes for runs P1 (dotted) and P2 (dashed), where 1980 values are defined as the 1975–1984 mean and 2000 values are the 1995–2004 mean. The green curve shows the equivalent 1980 to 2000 temperature change without the impacts of CFCs for run Cl1960 (green dash-dotted). The two red curves show the inferred temperature change caused by CFCs, obtained by subtracting the change for Cl1960 from the total changes in P1 and P2.

[42] The next aspect to consider is why the ozone decrease in the CCM is smaller than that in the CTM. This is most likely associated with the temperature-ozone feedback. The GCM run used to drive the CTM had no temperature trend, because it did not include any changes in ozone or GHGs. Ozone in the CTM decreases because of the increase in stratospheric halogen loading between 1980 and 2000 (the same scenario growth as used in the CCM runs). Because ozone has an inverse relationship with temperature [e.g., *Douglass et al.*, 1985] the GHG-induced stratospheric cooling should modulate the ozone decrease, meaning that the CTM is likely to overpredict the ozone change. In the CCM, the interaction of the ozone and GHGs with the GCM's radiation code means that proper account is taken of this feedback, so the ozone decrease between 1980 and 2000 is smaller than in the CTM. This can explain why the peak ozone loss in the CTM is larger than that in observations (Figure 9), but it does not explain why the loss in the CCM is smaller than that in observations. In the lower stratosphere the ozone change is similar in all three data sets.

[43] In summary, this section has used the time-slice runs of the GCM and CCM to examine the mechanisms of change (between 1980 and 2000) in the global thermal structure and ozone profile. The interdependence of ozone and temperature, through radiation transfer and the inverse-temperature dependence of kinetic reaction rates, mean that the feedbacks are important in moderating the coupled chemical and physical changes in the stratospheric state. Neglecting the GHG- and ozone-induced changes in temperature, ozone loss is overestimated in the middle-upper stratosphere.

6. Antarctic Ozone and the Polar Vortex

[44] The Antarctic ozone hole [*Farman et al.*, 1985] is one of the most prominent consequences of anthropogenic ozone destruction. Many GCMs and CCMs capture the basic dynamics of the Antarctic polar vortex, but undergo a late transition from winter to summer. This behavior has been related to inadequate representation of gravity wave drag [e.g., *Garcia and Boville*, 1994], but remains a problem in many present-day CCMs [*Eyring et al.*, 2006]. *Stolarski et al.* [2006b] document the late vortex breakdown in the GEOS CCM, at the same time showing that the morphology of the circulation associated with this breakdown is correctly captured. This circulation causes an ozone increase above the remnants of the ozone hole in late spring.

[45] This discussion of the Antarctic circulation first addresses an apparent contradiction in the model behavior. Despite the tendency for a delay in the vortex breakdown, there is too much year-to-year variability in the vortex structure compared to observations.

[46] The time-dependent structure of bias in the CCM is shown by statistics of daily values of zonal-mean zonal wind at 50 hPa, averaged for 40°S–80°S (Figure 12). The mean wind in the CCM is stronger than that in NCEP/NCAR reanalyses for much of the year: the reanalyses show negative values in summertime, while the simulation does not cross the zero line. The simulated winds show a bias of about 5 m/s between February and late June and during this period the mean simulated winds lie at the top edge of the envelope of analyzed winds (the range of both simulated and analyzed winds being about 10 m/s). The model attains its strongest mean westerlies about two weeks before the analyses; the slow decrease in mean simulated winds then falls in parallel with the analyzed values through parts of August and September, but through October and November the analyzed winds decrease in speed more quickly than the model, leading to the onset of the summertime bias. Although the mean winds are generally stronger in the CCM than in the analyses, the spread of values attained in the CCM is larger than in the real atmosphere. In particular, the envelope is larger in middle and late winter.

[47] *Newman et al.* [2001] demonstrated the dominant role of eddy forcing over the past weeks in determining the state of the stratosphere. Scatterplots of polar temperature versus the eddy heat flux through the tropopause have been used as a standard for evaluating this relationship in GCMs [*Austin et al.*, 2003; *Eyring et al.*, 2006]. Figure 13 shows such a scatterplots for runs P1 and P2, along with that for

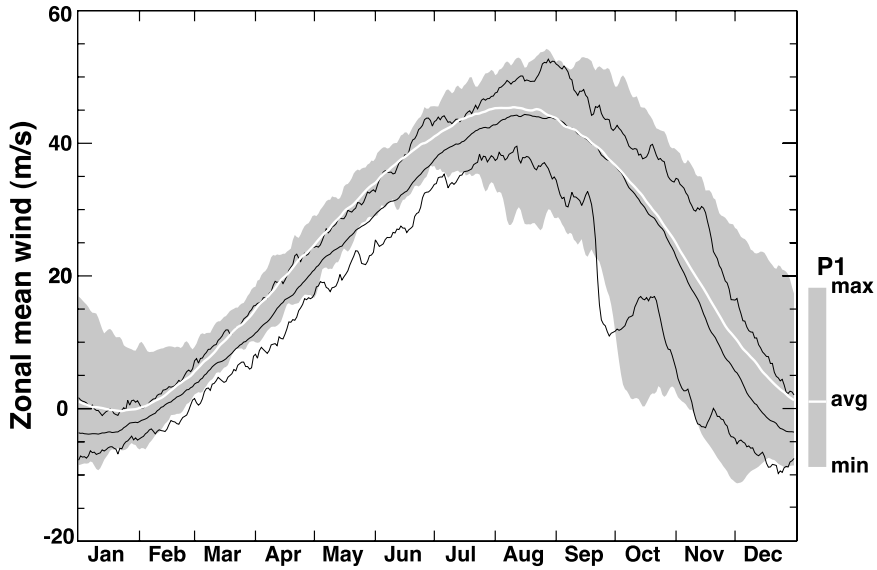

Figure 12. Time series of zonal-mean zonal wind at 50 hPa, averaged for 80°–40°S, for model run P1 and National Centers for Environmental Prediction/National Center for Atmospheric Research (NCEP/NCAR) reanalyses. The white curve shows the mean daily values for run P1, with gray shading delineating the range of values obtained for that day. The equivalent mean and envelope for the NCEP/NCAR analyses are shown by thick and thin black curves, respectively.

NCEP-NCAR reanalyses. This plot emphasizes that there are more warm Octobers in both simulations than in the reanalyses and that these warmer years are caused by higher-than-average wave activity. Figure 13 also shows that the model is biased cold in years when the heat flux is low, but tends to have smaller bias (even a warm bias in run P1) in years when the heat flux is high. These caveats need to be considered in the discussion of long-term changes.

[48] Figure 14 shows time series of polar (63°–90°S) ozone in October from observations and the three transient GEOS CCM simulations (P1, P2, and Cl1960). Over the period in which stratospheric chlorine loading increases, polar ozone values decrease from more than 300 DU before 1980 to less than 200 DU in the late 1990s. A similar decrease is shown in simulations P1 and P2. However, the high bias evident in early years substantially decreases in the period with high stratospheric chlorine. The absolute decrease in Antarctic springtime total ozone column is thus overestimated by 50–80% in these simulations.

[49] The omission of chlorine increases from run Cl1960 means that ozone remains high in the Antarctic vortex through the duration of the model run (Figure 14). There is a small increase in polar ozone in the run, likely induced by the inverse temperature dependence of ozone destruction: as temperatures decrease slightly owing to greenhouse-gas warming, the ozone destruction rate decreases and the concentrations increase.

[50] Deductions from observations suggest that the ozone hole leads to a cooling trend in the Antarctic spring [e.g., *Randel and Wu*, 1999]. Time series of Antarctic temperature at 50 hPa in October (Figure 15) reveal the behavior of the CCM. There is cooling in runs P1, P2 and Cl1960, but it is much stronger in P1 and P2 where ozone depletion occurs. Note that the two runs are biased cold compared to the GEOS-4 analyses, which are constrained by a few sondes and satellite observations in the Antarctic. The excessive year-to-year variability in the CCM is evident in this time series. In runs P1 and P2, the cooling is sufficiently large to support the formation of polar stratospheric clouds in the 1990s, which occur with substantial year-to-year variations in runs P1 and P2, but not in run Cl1960. The cold bias of the GEOS CCM in undisturbed years suggests that this may be an artifact of the model, but temperatures in analyses fall below 195 K in the middle-late 1990s.

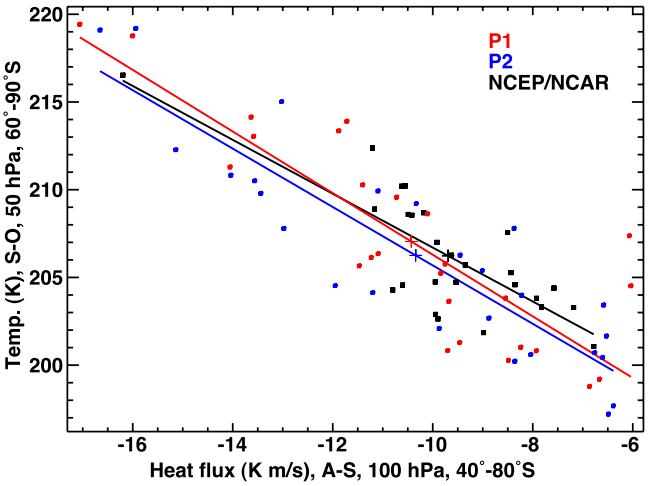

Figure 13. Scatterplot of the 100-hPa eddy heat flux versus the 50-hPa polar temperature for Antarctica in reanalysis (black dots) and model runs P1 (red dots) and P2 (blue dots). The 100-hPa eddy heat flux is averaged over the domain 80°–40°S from once daily values in August and September. The 50-hPa polar temperature is the 90°–60°S average for September and October.

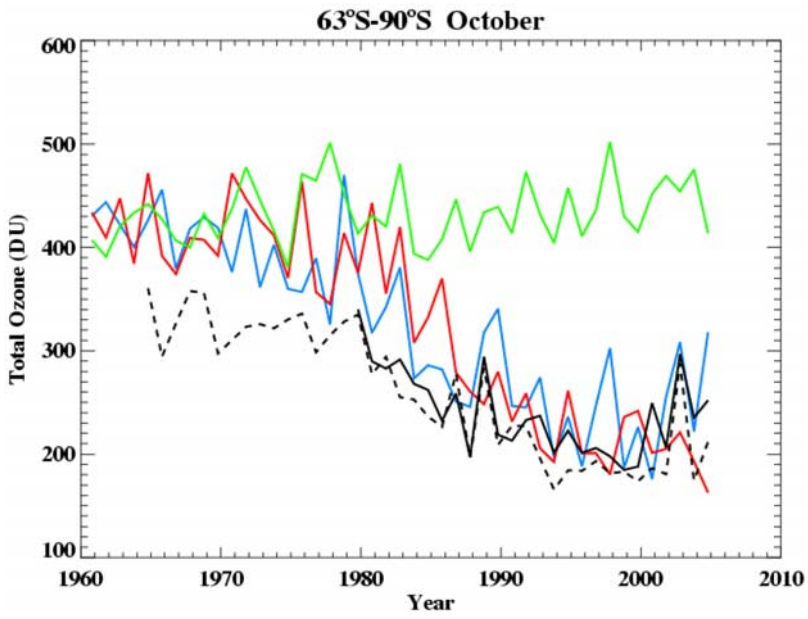

Figure 14. Time series of ozone in October in observations (black curves: solid for space-based data and dashed for ground-based), runs P1 (red curve) and P2 (blue curve), as well as run Cl1960 (green curve).

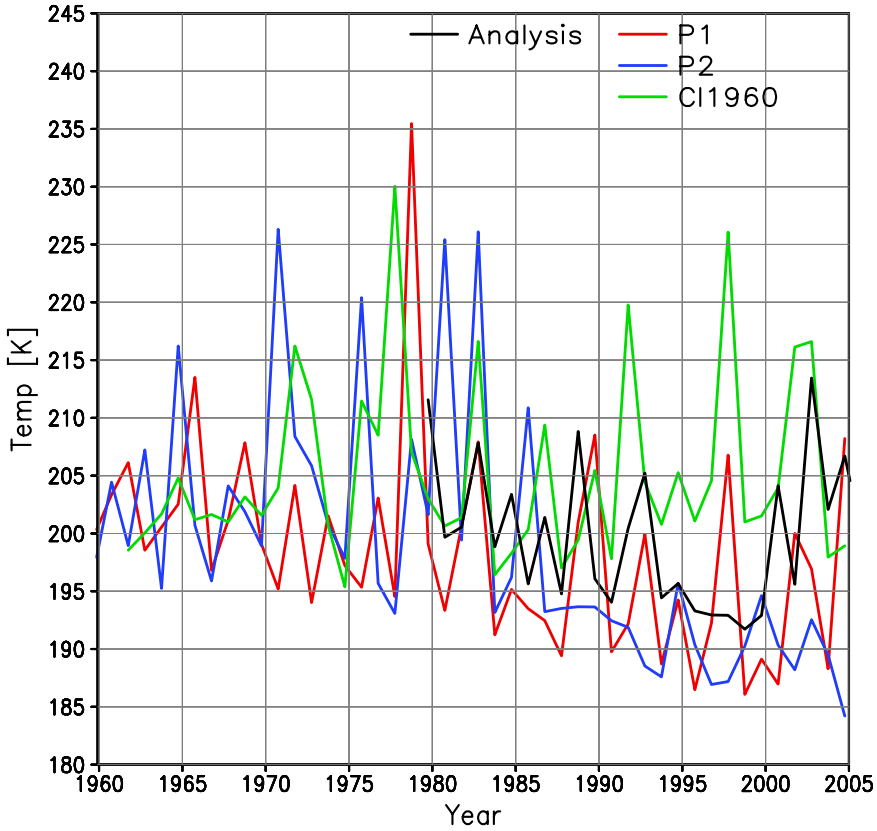

Figure 15. Time series of South Pole temperature (K) at 50 hPa in October between 1960 and 2004 in the GEOS CCM for model runs P1 (red curve), P2 (blue curve), and Cl1960 (green curve) and for GEOS-4 analyses (black curve).

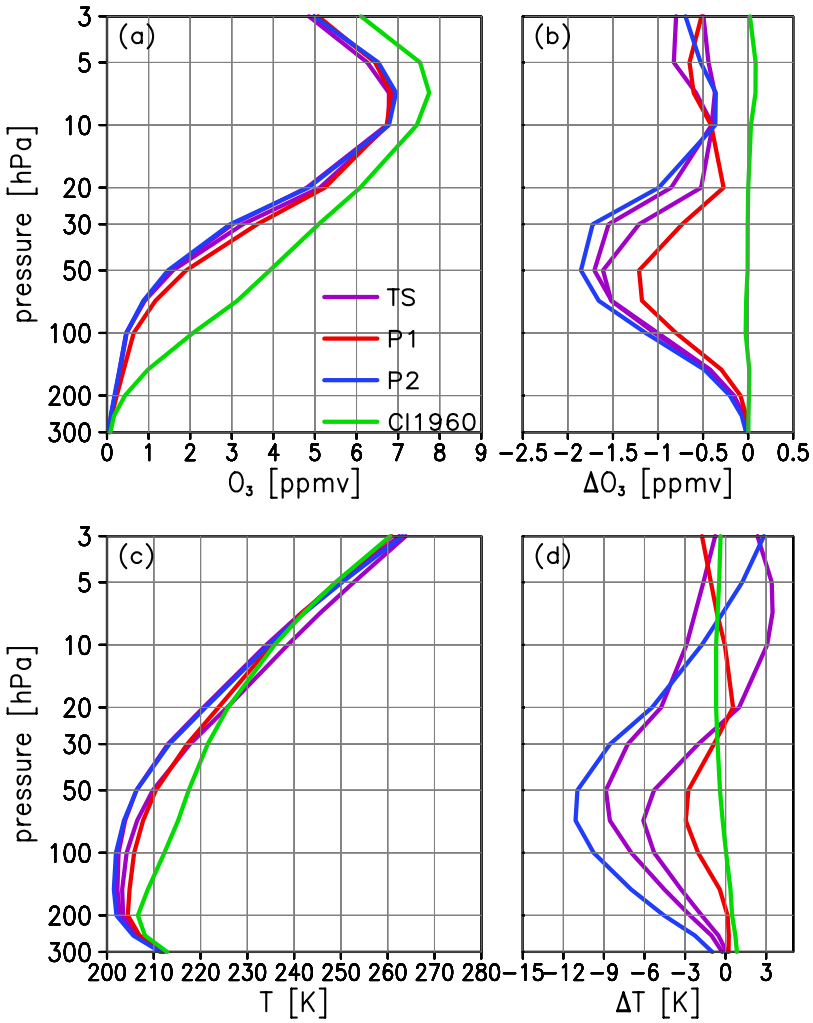

Figure 16. Ozone and temperature over Antarctica (60°–90°S mean) in October and their changes between 1980 and 2000 in the GEOS CCM. (a) Ozone (ppmv) averaged for 1995–2004 for runs P1 (red curve), P2 (blue curve), and Cl1960 (green curve) and for two non-overlapping 10-year averages of T2000 (violet curve). (b) The 2000 minus 1980 ozone differences (ppmv) for the three time-dependent runs (1980 values are 1975–1984 means). For the time-slice runs, two separate 10-year means for T1980 and T2000 were computed. (c, d) The equivalent plots for temperature (K).

[51] Quantitative estimates of the changes in ozone and temperature over Antarctica in the CCM are shown in Figure 16. All quantities are averaged between 60° and 90°S. The ozone profile (Figure 16a) shows substantial depletion in 2000 (the 1995–2004 average) in runs P1, P2, and T2000 compared to Cl1960. In the 200-30 hPa layer, temperatures in the three runs with depleted ozone are up to 10 K colder than in Cl1960 (Figure 16c). This demonstrates the direct impact of the chlorine loading on the ozone and temperature. The changes in ozone and temperature between 1980 and 2000 (Figures 16b and 16d) reveal the combined impacts of chlorine and GHG increases. There is a negligible perturbation to the ozone column in run Cl1960 and only very slight cooling (up to about 1 K) over Antarctica. The ozone depletion between 1980 and 2000 peaks near 50 hPa and is bracketed by P1 (1.2 ppmv decrease) and P2 (1.8 ppmv decrease). The two estimates from runs T1980 and T2000 use separate 10-year averages (years 5–14 and 15–24) in each run, so they are approximately independent. Corresponding temperature changes show peak cooling of 3 K in P1 and 11 K in P2 near 70 hPa, with all runs showing some degree of warming in the upper stratosphere which is due increased downwelling [*Stolarski et al.*, 2006b]. These ozone and temperature changes in the low stratosphere over Antarctica are broadly consistent with those computed by *Langematz et al.* [2003], *Manzini et al.* [2003], and *Braesicke et al.* [2006]. However, the various runs show a large discrepancy in the magnitude of ozone loss and temperature decrease between 1980 and 2000. This is because the Antarctic stratosphere displays too much dynamical variability in the GCM/CCM with more disturbed winters than have been observed in the past few decades.

[52] Very similar ozone and temperature changes are obtained from GCM runs using ozone from the CTM, but not from those using observed ozone. Four of the twelve years in run G2000/OBSO3 contain major warmings over Antarctica, which leads to a net warming between the 1980

and 2000 experiments. This abundance of warm Antarctic winters in this model is an adverse feature that impacts interpretation of the results.

7. Conclusions and Discussion

[53] This manuscript has discussed the performance of the GEOS CCM when integrated for 1950–2005, forced by SST/ice boundary conditions derived from observations and by emitted greenhouse gases and chlorine-containing trace gases. The foci of the work were validation of ozone and temperature against observations, evaluation of the feedbacks in the CCM, and comparisons with earlier studies of ozone impacts on the stratosphere. Several aspects of one run (P1) of this CCM were evaluated alongside other CCMs in the work of *Eyring et al.* [2006], which showed that for most metrics the model generally falls well within the range of other CCMs. An important underlying aspect of this model is the realism of the transport using the *Lin* [2004] dynamical core, which has not been described in detail in this study. Some aspects of transport in this model were evaluated by *Eyring et al.* [2006], and other aspects will be described in more detail in future studies.

[54] 1. In terms of temperature-ozone coupling, the following conclusions were reached: Total ozone in the chemistry code is biased high compared to observations. This is mainly owing to high concentrations in the low stratosphere. The bias is more pronounced in the era before significant stratospheric chlorine loading. The dominance of chlorine-induced ozone loss in recent years suggests that another mechanism for ozone removal in the low stratosphere is too weak.

[55] 2. The dependence of the ozone bias on the chlorine loading means that the chlorine-induced changes in ozone between 1980 and 2000 are too large in the model, by a factor of about 60–80% in the Antarctic spring.

[56] 3. There is a low ozone bias in the upper stratosphere of the CTM/CCM.

[57] 4. The thermal structure of the GCM/CCM is strongly constrained by ozone. The low ozone bias in the upper stratosphere leads to a cooler stratopause in CCM and GCM simulations with simulated ozone than in GCM runs with observed ozone.

[58] 5. The modeled stratopause temperature is too warm when the GCM is run with observed ozone, but is closer to that observed with ozone from the CTM. The CCM stratopause temperature is close to that observed. This means that there is a discrepancy between our knowledge (based on observations) of the structure of the upper stratosphere and our understanding of processes that cause this structure.

[59] 6. The high bias in lower stratospheric ozone in the CTM/CCM leads to a warm bias in the thermal structure of the model. Absorption by ozone of upwelling infrared radiation plays an important role in this temperature bias.

[60] 7. In the middle stratosphere (5–10 hPa), the interactive computations, where temperature and ozone interact, yield a better simulation of ozone than in the CTM constrained with GCM temperatures. The profile remains somewhat biased in the CCM. This illustrates the importance of the temperature feedback in the chemistry-radiation computations.

[61] 8. The model predicts ozone-forced changes in global-mean temperature between 1980 and 2000 that are broadly consistent with observations and other models. The GCM response to imposed ozone changes is at the "low end" of previous GCM studies. The CCM responds in a manner similar to the GCM with ozone changes imposed from either observations or the CTM.

[62] 9. Changes in greenhouse gases between 1980 and 2000 lead to a cooling of about 1.3 K near 1 hPa, compared to an ozone impact of about 1.5 K.

[63] 10. The modeled Antarctic vortex is, in most years, too cold and too persistent. However, the GCM and CCM both undergo too many major disturbances in the middle-late winter, meaning that the interannual variability of the polar vortex and ozone loss are too large compared to the real atmosphere.

[64] 11. The excess variability of the Antarctic vortex leads to a large spread in estimates of Antarctic ozone loss between 1980 and 2000 in the various simulations analyzed. Estimates of ozone-induced cooling at 70 hPa in the Antarctic vortex ranges from 3–12 K in the decadal averages used here. Runs P1 and P2 display the smallest and largest changes, bracketing the estimates from time-slice model integrations.

[65] These conclusions highlight the many of the strengths and weaknesses of the GEOS CCM. The two major weaknesses are the anomalous nature of the Antarctic vortex (too cold and long-lived, but with too many disturbed winters) and the high bias in total ozone. The ozone bias and its relationship to chlorine loading impacts the magnitude of trends in the model, as well as leading to a warm bias in the lower stratospheric temperature. These are caveats that must be considered as the CCM is used for examination of ozone and temperature changes through the twenty-first century. Despite these weaknesses, the CCM displays integrity in its ability to represent aspects of the global coupling between ozone and temperature. Further analyses of these and several other GEOS CCM runs will help understand the processes that maintain the interactive composition and circulation of the middle atmosphere, the links between ozone change and the troposphere, and the likely future evolution of the chemical and physical climate of the atmosphere. These analyses will include more detailed study of meteorology and transport than has been given here, where the focus has been on the temperature-ozone coupling.

[66] **Acknowledgments.** Thanks to NASA for high-performance computing resources on "Project Columbia" and staff at NAS for assistance in keeping the models running. Many colleagues have contributed to different aspects of software development and model maintenance. Ulrike Langematz provided her ozone data sets for our use. We thank Michele Rienecker of the GMAO for her continuing encouragement and support and Don Anderson of NASA's MAP Program for funding. Finally, we express our appreciation to Darryn Waugh and the three anonymous peer reviewers, whose comments led to an improved paper, and to John Austin, for his efficient editorial work at *JGR-Atmospheres*. This is contribution number 2 of the Goddard Chemistry/Climate Modeling Project.

References

Austin, J., and R. J. Wilson (2006), Ensemble simulations of the decline and recovery of stratospheric ozone, *J. Geophys. Res.*, *111*, D16314, doi:10.1029/2005JD006907.

Austin, J., et al. (2003), Uncertainties and assessments of chemistry-climate models of the stratosphere, *Atmos. Chem. Phys.*, *3*, 1–27.

Bloom, S., et al. (2005), The Goddard Earth Observation System Data Assimilation System, GEOS DAS version 4.0.3: Documentation and validation, *NASA Tech. Memo., NASA TM-2005-104606*, vol. 26, 166 pp.
Boer, G. J., et al. (1992), Some results from an intercomparison of the climates simulated by 14 atmospheric general circulation models, *J. Geophys. Res.*, *97*, 12,771–12,786.
Bosilovich, M. G., S. D. Schubert, and G. K. Walker (2005), Global changes of the water cycle intensity, *J. Clim.*, *18*, 1591–1608.
Braesicke, P., and J. A. Pyle (2004), Sensitivity of dynamics and ozone to different representations of SSTs in the unified model, *Q.J.R. Meteorol. Soc.*, *130*, 2033–2045.
Braesicke, P., M. M. Hurwitz, and J. A. Pyle (2006), The stratospheric response to changes in ozone and carbon dioxide as modeled with a GCM including parameterized ozone chemistry, *Meteorol. Z.*, *15*(3), 1–12.
Charlton, A. J., L. M. Polvani, J. Perlwitz, F. Sassi, E. Manzini, K. Shibata, S. Pawson, J. E. Nielsen, and D. Rind (2007), A new look at stratospheric sudden warmings: part II. Evaluation of numerical model simulations, *J. Clim.*, *20*, 470–488.
Considine, D. B., A. R. Douglass, P. S. Connell, D. E. Kinnison, and D. A. Rotman (2000), A polar stratospheric cloud parameterization for the global modeling initiative three-dimensional model and its response to stratospheric aircraft, *J. Geophys. Res.*, *105*(D3), 3955–3974.
Considine, D. B., S. R. Kawa, M. R. Schoeberl, and A. R. Douglass (2003), N_2O and NO_y observations in the 1999/2000 arctic polar vortex: Implications for transport processes in a CTM, *J. Geophys. Res.*, *108*(D5), 4170, doi:10.1029/2002JD002525.
de Grandpré, J., S. R. Beagley, V. I. Fomichev, E. Griffioen, J. C. McConnell, A. S. Medvedev, and T. G. Shepherd (2000), Ozone climatology using interactive chemistry: Results from the Canadian Middle Atmosphere Model, *J. Geophys. Res.*, *105*(D21), 26,475–26,492.
Douglass, A. R., and S. R. Kawa (1999), Contrast between 1992 and 1997 high-latitude spring Halogen Occultation Experiment observations of lower stratospheric HCl, *J. Geophys. Res.*, *104*, 18,739–18,754.
Douglass, A. R., R. B. Rood, and R. S. Stolarski (1985), Interpretation of ozone-temperature correlations: 2. Analysis of SBUV ozone data, *J. Geophys. Res.*, *90*, 10,693–10,708.
Douglass, A. R., C. J. Weaver, R. B. Rood, and L. Coy (1996), A three-dimensional simulation of the ozone annual cycle using winds from a data assimilation system, *J. Geophys. Res.*, *101*(D1), 1463–1474.
Douglass, A. R., M. R. Schoeberl, R. B. Rood, and S. Pawson (2003), Evaluation of transport in the lower tropical stratosphere in a global chemistry and transport model, *J. Geophys. Res.*, *108*(D9), 4259, doi:10.1029/2002JD002696.
Eyring, V., et al. (2006), Assessment of temperature, trace species, and ozone in chemistry-climate model simulations of the recent past, *J. Geophys. Res.*, *111*, D22308, doi:10.1029/2006JD007327.
Farman, J. C., B. G. Gardiner, and J. D. Shanklin (1985), Large losses of total ozone in Antarctica reveal seasonal ClO_x/NO_x interaction, *Nature*, *315*, 207–210.
Fels, S. B., J. D. Mahlman, M. D. Schwarzkopf, and R. W. Sinclair (1980), Stratospheric sensitivity to perturbations in ozone and carbon dioxide: Radiative and dynamical response, *J. Atmos. Sci.*, *37*, 2265–2297.
Fioletov, V., G. Bodeker, A. Miller, R. McPeters, and R. Stolarski (2002), Global and zonal total ozone variations estimated from ground-based and satellite measurements: 1964–2000, *J. Geophys. Res.*, *107*(D22), 4647, doi:10.1029/2001JD001350.
Forster, P. M. D., and K. P. Shine (1997), Radiative forcing and temperature trends from stratospheric ozone changes, *J. Geophys. Res.*, *102*, 10,841–10,855.
Garcia, R. R., and B. A. Boville (1994), Downward control of the mean meridional circulation and temperature distribution of the polar winter stratosphere, *J. Atmos. Sci.*, *51*, 2238–2245.
Garcia, R. R., and S. Solomon (1985), The effect of breaking gravity waves on the dynamics and chemical composition of the mesosphere and lower thermosphere, *J. Geophys. Res.*, *90*, 3850–3868.
Hare, S. H. E., L. J. Gray, W. A. Lahoz, A. O'Neill, and L. Steenman-Clark (2004), Can stratospheric temperature trends be attributed to ozone depletion?, *J. Geophys. Res.*, *109*, D05111, doi:10.1029/2003JD003897.
Hitschfeld, W., and J. T. Houghton (1961), Radiative transfer in the lower stratosphere due to the 9.6 micron band of ozone, *Q.J.R. Meteorol. Soc.*, *83*, 562–577.
Holton, J. R., P. H. Haynes, M. E. McIntyre, A. R. Douglass, R. B. Rood, and L. Pfister (1995), Stratosphere-troposphere exchange, *Rev. Geophys.*, *33*, 403–439.
Kiehl, J. T., J. J. Hack, G. B. Bonan, B. A. Boville, D. L. Williamson, and P. J. Rasch (1998), The National Center for Atmospheric Research Community Climate Model: CCM3, *J. Clim.*, *11*, 1131–1149.
Langematz, U. (2000), An estimate of the impact of observed ozone losses on stratospheric temperature, *Geophys. Res. Lett.*, *27*, 2077–2080.
Langematz, U., M. Kunze, K. Krueger, K. Labitzke, and G. L. Roff (2003), Thermal and dynamical changes of the stratosphere since 1979 and their link to ozone and CO_2 changes, *J. Geophys. Res.*, *108*(D1), 4027, doi:10.1029/2002JD002069.
Lin, S.-J. (2004), A vertically Lagrangian finite-volume dynamical core for global models, *Mon. Weather Rev.*, *132*, 2293–2307.
Lin, S. J., and R. B. Rood (1996), Multidimensional flux form semi-Lagrangian transport schemes, *Mon. Weather Rev.*, *124*, 2046–2070.
Lin, S. J., and R. B. Rood (1997), An explicit flux form semi-Lagrangian shallow-water model on the sphere, *Q.J.R. Meteorol. Soc.*, *123*, 2477–2498.
Logan, J. A. (1999), An analysis of ozonesonde data for the troposphere: Recommendations for testing 3—D models and development of a gridded climatology for tropospheric ozone, *J. Geophys. Res.*, *104*(D13), 16,115–16,150.
Manzini, E., B. Steil, C. Brühl, M. A. Giorgetta, and K. Krüger (2003), A new interactive chemistry-climate model: 2. Sensitivity of the middle atmosphere to ozone depletion and increase in greenhouse gases and implications for recent stratospheric cooling, *J. Geophys. Res.*, *108*(D14), 4429, doi:10.1029/2002JD002977.
Newman, P. A., E. Nash, and J. E. Rosenfeld (2001), What controls the temperature of the arctic stratosphere during spring?, *J. Geophys. Res.*, *106*, 19,999–20,010.
Olsen, M. A., M. R. Schoeberl, and J. E. Nielsen (2007), Response of stratospheric circulation and stratosphere-troposphere exchange to changing sea surface temperatures, *J. Geophys. Res.*, *112*, D16104, doi:10.1029/2006JD008012.
Pawson, S. (1992), Underestimates of O3 9.6 micron heating rates as a cause of the cold bias in the low tropical stratosphere of GCMs, *Ann. Geophys.*, *10*, 619–624.
Pawson, S., et al. (2000), The GCM-Reality Intercomparison Project for SPARC: Scientific issues and initial results, *Bull. Am. Meteorol. Soc.*, *81*, 781–796.
Ramaswamy, V., and M. D. Schwarzkopf (2002), Effects of ozone and well-mixed gases on annual-mean stratospheric temperature trends, *Geophys. Res. Lett.*, *29*(22), 2064, doi:10.1029/2002GL015141.
Randel, W. J., and F. Wu (1999), Cooling of the Arctic and Antarctic stratospheres due to ozone depletion, *J. Clim.*, *12*, 1467–1479.
Rayner, N. A., D. E. Parker, E. B. Horton, C. K. Folland, L. V. Alexander, D. P. Rowell, E. C. Kent, and A. Kaplan (2003), Global analyses of sea surface temperature, sea ice, and night marine air temperature since the late nineteenth century, *J. Geophys. Res.*, *108*(D14), 4407, doi:10.1029/2002JD002670.
Rood, R. B., A. R. Douglass, M. C. Cerniglia, and W. G. Read (1997), Synoptic-scale mass exchange from the troposphere to the stratosphere, *J. Geophys. Res.*, *102*(D19), 23,467–23,486.
Rosier, S. M., and K. P. Shine (2000), The effect of two decades of ozone change on stratospheric temperature as indicated by a general circulation model, *Geophys. Res. Lett.*, *27*, 2617–2620.
Sander, S. P., et al. (Eds.) (2003), *Chemical Kinetics and Photochemical Data for Use in Atmospheric Studies*, *JPL Publ.*, 02–25.
Santer, B. D., et al. (2003), Behavior of tropopause height and atmospheric temperature in models, reanalyses, and observations: Decadal changes, *J. Geophys. Res.*, *108*(D1), 4002, doi:10.1029/2002JD002258.
Sassi, F., D. Kinnison, B. A. Boville, R. R. Garcia, and R. Roble (2004), Effect of El Niño-Southern Oscillation on the dynamical, thermal, and chemical structure of the middle atmosphere, *J. Geophys. Res.*, *109*, D17108, doi:10.1029/2003JD004434.
Sassi, F., B. A. Boville, D. Kinnison, and R. R. Garcia (2005), The effects of interactive ozone chemistry on simulations of the middle atmosphere, *Geophys. Res. Lett.*, *32*, L07811, doi:10.1029/2004GL022131.
Schoeberl, M. R., A. R. Douglass, Z. Zhu, and S. Pawson (2003), A comparison of the lower stratospheric age spectra derived from a general circulation model and two data assimilation systems, *J. Geophys. Res.*, *108*(D3), 4113, doi:10.1029/2002JD002652.
Simmons, A. J., and R. Strüfing (1983), Numerical forecasts of stratospheric warming events using a model with hybrid vertical coordinate, *Q. J. R. Meteorol. Soc.*, *109*, 81–111.
Stolarski, R. S., and S. M. Frith (2006), Search for evidence of a trend slowdown in the long-term TOMS/SBUV total ozone data record: The importance of instrument drift uncertainty, *Atmos. Chem. Phys.*, *6*, 4057–4065.
Stolarski, R. S., A. R. Douglass, S. Steenrod, and S. Pawson (2006a), Trends in stratospheric ozone: Lessons learned from a 3D chemistry transport model, *J. Atmos. Sci.*, *63*, 1028–1041.
Stolarski, R. S., A. R. Douglass, M. Gupta, P. A. Newman, S. Pawson, M. R. Schoeberl, and J. E. Nielsen (2006b), An ozone increase in the Antarctic summer stratosphere: A dynamical response to the ozone hole, *Geophys. Res. Lett.*, *33*, L21805, doi:10.1029/2006GL026820.

World Meteorological Organization (2003), Scientific assessment of ozone depletion: 2002, *Rep. 47*, 498 pp., Global Ozone Res. and Monit. Proj., Geneva.

A. R. Douglass, S. M. Frith, P. A. Newman, and R. S. Stolarski, Atmospheric Chemistry and Dynamics Branch, NASA Goddard Space Flight Center, Greenbelt, MD 20771, USA.

M. L. Gupta, Federal Aviation Administration, Washington, D.C., 20591, USA.

J. E. Nielsen and S. Pawson, Global Modeling and Assimilation Office, Mail Code 610.1, NASA Goddard Space Flight Center, Greenbelt, MD 20771, USA. (steven.pawson@nasa.gov)